

APPLICATIONS OF ADVANCED ELECTRONIC MATERIALS: InSe SYSTEM $(\text{In}_{10}\text{Se}_{90})_{100-x}\text{Pb}_x$ WITH $x = 0, 2, 5, 10$ FOR PCRAM APPLICATIONS

M. D. SHARMA*, N. GOYAL

**Department of Physics, Centre of Advanced Study in Physics, Panjab University Chandigarh, India*

This manuscript describes the preparation of pure InSe Chalcogenide glasses along with its Pb doped samples $(\text{In}_{10}\text{Se}_{90})_{98}\text{Pb}_2$, $(\text{In}_{10}\text{Se}_{90})_{95}\text{Pb}_5$ and $(\text{In}_{10}\text{Se}_{90})_{90}\text{Pb}_{10}$ having different weighted % as 2 at. wt%, 5 at. wt% and 10 at. wt% respectively using melt and quench procedure. The prepared samples were structurally, morphologically and optically characterized using various techniques such as UV-Vis Spectroscopy, Field Emission-Scanning Electron Microscopy (FE-SEM) and X-Ray diffraction (XRD). XRD results unfold that with the addition of Pb in amorphous InSe incorporated crystalline nature in the obtained doped glasses with maximum crystallinity observed with maximum doping percentage i.e. 10 at. wt%. FE-SEM micrographs showed that undoped InSe nanoparticles were spherical in shape. However with Pb addition, the shape become distorted and resulted in agglomeration at maximum doping percentage of 10 at. wt%. The optical properties were studied from UV-Vis analysis and it was emphasised that with the addition of Pb in pure InSe, the band gap of obtained glasses follow decreasing trend with least value ($E_g = 1.55$ eV) obtained in maximum doped percentage of Pb. The dielectric measurements of pure as well as doped samples were studied and various parameters such as dielectric constant (both real and imaginary) and dielectric loss were studied as a function of frequency that varies from 50 Hz to 5 MHz.

(Received January 20, 2018; Accepted April 21, 2018)

Keywords: Indium, Selenium, Antimony, Doping, X-Ray Diffraction, Band Gap

1. Introduction

Chalcogenide glasses (ChGs) are comprised of group VI elements (S, Se, and Te) with the incorporation of foreign elements such as Sb, Ga, In, Ge, etc. They contain single or multiple chalcogen atoms covalently attached to lattice builders. Research in this field has been stimulated by the unique properties of these glasses, started around sixty years ago especially because of their ease of fabrication for bulk and thin films formation [1,2]. They have flexible structure, in such a way that each atom can adjust according to the valency of its neighbouring element.

Some of the very exciting properties of ChGs like photosensitivity are useful in the area of linear and non-linear optics.

These materials can be employed in various domains of technology. Their implementation in memory devices and optical fibres is majorly significant. Other applications include photolithography, solar cells, laser diodes and xerography [3,4]. Very less research has been carried out on material properties of layered chalcogenides, such as III-VI compounds (GaSe, InSe etc). These selenide glasses are particularly fascinating due to their broad transparency in the mid infrared region and suitable thermal stability. Amongst them, InSe (Indium selenide) is of considerable interest owing to its intriguing polymorphism and potential applications.

Indium Selenide (InSe) is a group of layered semiconductors in which each layer consist of a honeycomb matrix comprising four covalently attached Se-In-In-Se atomic planes. Bulk InSe is a direct band gap semiconductor (~ 1.25 eV at room temperature) that is appealing due to

* Corresponding author: manishdevsharma@yahoo.com

its optical properties, structural transformations under pressure, good quality thin film preparation, lithium batteries, and solar cells with an efficiency of 11% [5].

In 1968, Ovshinsky made known the concept of utilising phase change mechanism of certain chalcogenides for storage media. These memory devices based on resistive phase change property are faster in writing/reading process, enhanced endurance, and are easier to fabricate than conventional transistor-based non-volatile memories. Second generation solar cells (CIGS) also called thin-film solar cells but it's had lower efficiency and increased the toxicity which is overcome by ultra- thin CZTS solar cell. The active buffer layer in these solar cells is formed by InSe material.

2. Experimental Details

A novel composition of $(\text{In}_{10}\text{Se}_{90})_{100-x}\text{Pb}_x$ materials where $x = (0, 2, 5, 10)$ at. wt% has been explored for various material properties. The polycrystalline bulk samples were prepared with the conventional melt and quench procedure. Raw materials purchased from sigma Aldrich were weighed in proper stoichiometric proportion and vacuum sealed in a quartz ampoule. The ampoules were annealed at 1000°C for 6 hours and rapidly quenched in ice water. The bulk powder obtained was further processed in a thermal evaporation chamber to obtain amorphous thin films on glass substrate.

2.1. Preparation of bulk materials

The Polycrystalline bulks of $(\text{In}_{10}\text{Se}_{90})_{100-x}\text{Pb}_x$ with $x=0, 2, 5$ at. wt% were obtained with conventional melt-quench procedure as shown in Fig. 1. Powdered forms of pure Indium, Selenium and lead were weighed according to three Stoichiometric compositions: $\text{In}_{10}\text{Se}_{90}$, $(\text{In}_{10}\text{Se}_{90})_{98}\text{Pb}_2$, $(\text{In}_{10}\text{Se}_{90})_{95}\text{Pb}_5$ and $(\text{In}_{10}\text{Se}_{90})_{95}\text{Pb}_{10}$. These compounds were then sealed in quartz ampoules at 10^{-5} Mbar. The ampoules were heated in a muffle furnace at 900°C for 12 hours and immediately quenched in ice water. The ingots obtained were again powdered to obtain the bulk samples.

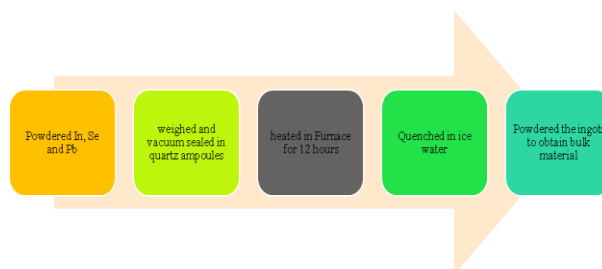


Fig.1. Experimental preparation of bulk material

2.2. Preparation of Thin Films

Thin films can be produced by physical method, in which materials are thermally evaporated to be deposited on the substrate. Vacuum thermal evaporation technique has been employed to manufacture thin films of all the InSe compositions on glass substrates. The process is carried out in vacuum at 10^{-5} Mbar pressure.

3. Results and discussion

The microstructures of InSe and Pb doped InSe thin films namely $\text{In}_{10}\text{Se}_{90}$, $(\text{In}_{10}\text{Se}_{90})_{98}\text{Pb}_2$, $(\text{In}_{10}\text{Se}_{90})_{95}\text{Pb}_5$ and $(\text{In}_{10}\text{Se}_{90})_{95}\text{Pb}_{10}$. with 2 at. wt%, 5 at. wt% and 10 at. wt% of lead respectively were studied structurally, morphologically, optically and electrically. The structural study was done by X-Ray Diffraction (XRD) technique using Panalytical's X'Pert Pro

X-ray diffractometer operating at 45 kV and 40 mA with Cu-K α radiation having 2θ ranging from 10° to 80° . The particle size and shape was calculated using HITACHI Field effect Scanning Electron Microscope (FE-SEM) SU8010 model. The transmission spectra of pure InSe and lead doped InSe were measured using UV-Vis spectrometer (Perkin Elmer LAMBDA 750) in the transmission range of 400 nm - 4000 nm at room temperature. The electrical properties were measured using two probe process with Keithley 6517A electrometer and DNM-121 nanoammeter as voltage source and current measuring source respectively. The Capacitance-voltage measurements were performed using HIOKI 3532 LCR Hi-Tester with frequency range of 50 Hz to 5 MHz.

3.1. Structural Characterization

3.1.1. X-Ray Diffraction

The X-Ray diffractogram of pure In₁₀Se₉₀ and lead doped In₁₀Se₉₀ i.e. (In₁₀Se₉₀)₉₈Pb₂, (In₁₀Se₉₀)₉₅Pb₅ and (In₁₀Se₉₀)₉₅Pb₁₀ were exhibited in Figure 3. Here it was clearly observed that pure InSe nanoparticles were amorphous in nature with characteristic peak observed at $2\theta = 23.2^\circ$ corresponding to (004) crystal plane of pure InSe. The average crystallite size was calculated as 14.7 nm using Debye-Scherrer equation [7]:

$$D = k\lambda/\beta\cos\theta \quad (1)$$

where k presents the factor for mean crystallite, β (in radians) is the full width at half maxima (FWHM) of crystalline planes. The d-spacing equivalent to maximum crystalline peak was calculated using Bragg's relation:

$$n\lambda = 2d\sin\theta \quad (2)$$

where n is an integer, θ is the angle formed between incident and reflected rays and λ is 1.54 Å for Cu target. The d-spacing corresponding to crystalline peak $2\theta = 23.2^\circ$ was 3.83 Å. The XRD pattern for Pb doped InSe nanoparticles i.e. In₁₀Se₉₀, were displayed in Fig. 2 (b) – (d). The pattern vividly proved that with the addition of Pb in InSe system, the amorphous nature of the sample was converted into crystalline and the degree of crystallinity was further enhanced with increase in wt% of Pb. From the XRD spectrum, it was found that the characteristic peak of InSe corresponding to crystalline plane (004) was present in all the samples but in lead doped samples along with it there exist three more peaks at $2\theta = 25.4^\circ$, 29.1° and 42.1° corresponding to (220), (311) and (440) crystal planes respectively [8]. The crystallite size and d-spacing in (In₁₀Se₉₀)Pb₁₀ i.e. with 10 at. wt% Pb corresponding to (311) plane were found to be 14.5 nm and 3.06 Å respectively.

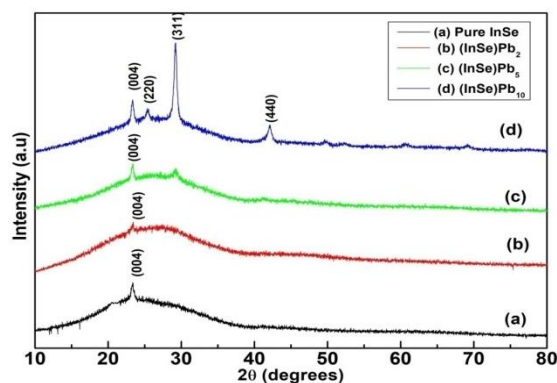
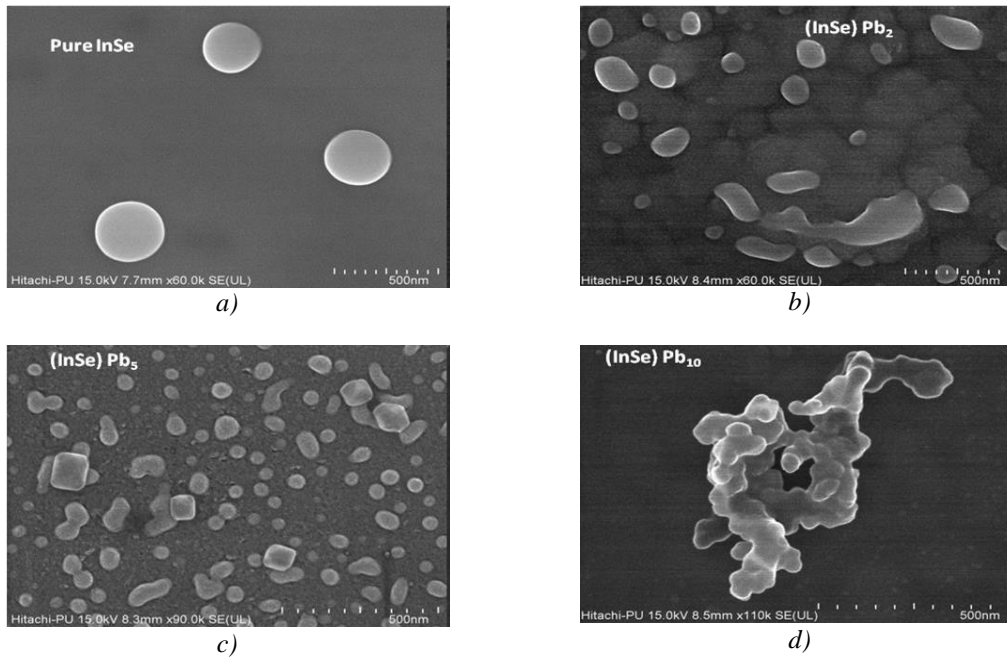


Fig.2. XRD of (a) Pure InSe and (b) - (d) different weighted lead doped InSe

3.1.2 Field Effect Scanning Electron Microscopy

The Field Effect Scanning Electron Microscopy (FE-SEM) micrographs of pure $(\text{In}_{10}\text{Se}_{90})_{98}\text{Pb}_2$, $(\text{In}_{10}\text{Se}_{90})_{95}\text{Pb}_5$ and $(\text{In}_{10}\text{Se}_{90})_{95}\text{Pb}_{10}$ samples were displayed in Fig. 3. From Fig. 3 (a) it was found that pure InSe particles were spherical in shape and their size lies in nanometre range. However with the addition of Pb in the Pure InSe sample, the shape of the thus formed sample particles gets distorted as exhibited by Fig. 3 (b), (c) and (d). It was also emphasised that with the addition of higher atomic wt% of Pb in InSe sample the particles undergo agglomeration and at atomic wt% = 10%, the maximum agglomeration was observed as seen from Fig. 3 (d).



*Fig.3. FE-SEM Micrograph of
 a) pure InSe, b) doped InSe with 2% Pb,
 c) doped InSe with 5% Pb, d) doped InSe with 10% Pb*

3.2. Optical Characterization: UV-Vis spectroscopy

Chalcogenide glasses are within the scope of knowledge to be direct band gap semiconductors. The plots of $(\alpha h\nu)^{1/2}$ vs $h\nu$ for $\text{In}_{10}\text{Se}_{90}$ and lead doped $\text{In}_{10}\text{Se}_{90}$ i.e. $(\text{In}_{10}\text{Se}_{90})_{98}\text{Pb}_2$, $(\text{In}_{10}\text{Se}_{90})_{95}\text{Pb}_5$ and $(\text{In}_{10}\text{Se}_{90})_{95}\text{Pb}_{10}$ glasses are displayed in Fig. 4 ((a)- (d)).

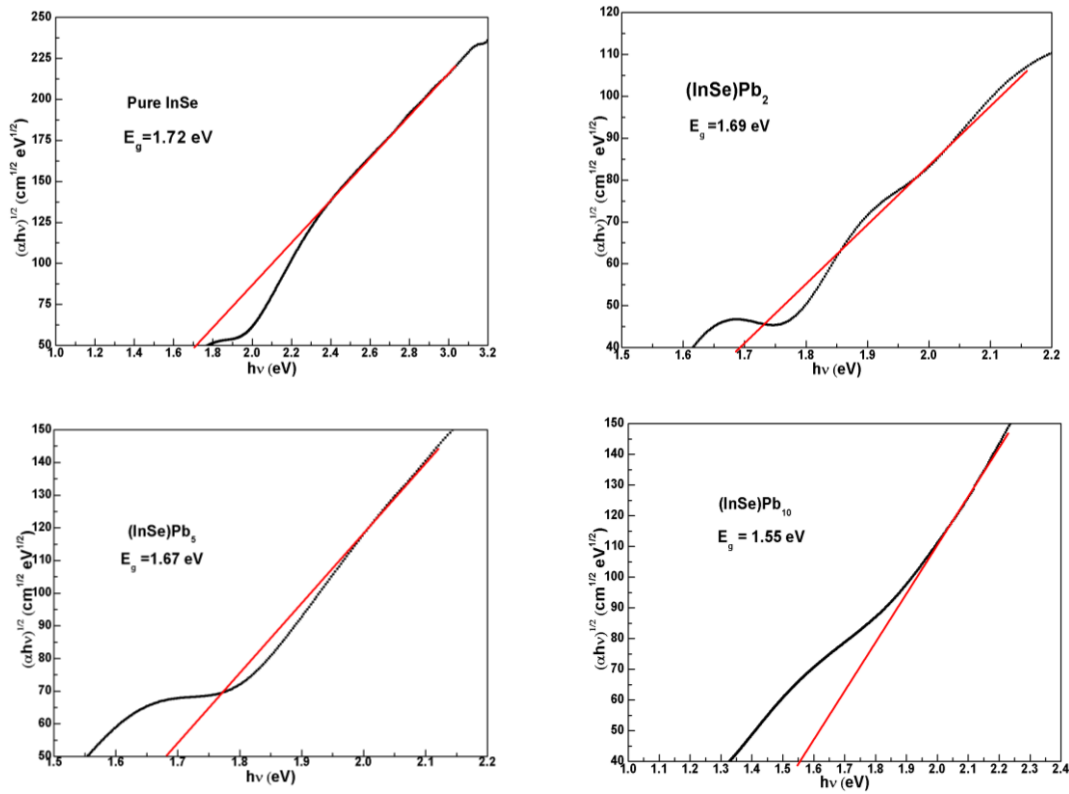


Fig.4. Plots of $(\alpha hv)^{1/2}$ vs hv for InSe and different weighted lead doped InSe Chalcogenide glasses.

The band gap of a material can be determined using the absorption peak corresponding to transition from valence band to conduction band. The relationship between absorption coefficient (α) and incident energy ($h\nu$) from the power law given by Tauc can be written as :

$$\alpha = \frac{A(h\nu - E_g)^n}{h\nu} \quad (3)$$

Where A is constant and E_g is the optical band gap. The n may have values 1/2, 2, 3/2 and 3, depending on the type of transition and it corresponds to allowed direct, allowed indirect, forbidden direct and forbidden indirect transitions respectively [9].

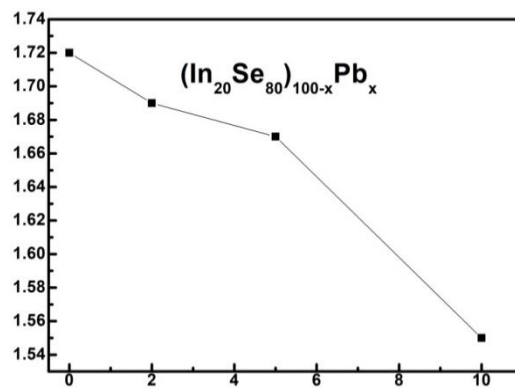


Fig.5. Variation of E_g with different wt% of Pb in InSe Chalcogenide glasses.

The value of E_g can be estimated by extrapolating the straight line portion of $(ah\nu)^{1/n}$ vs $h\nu$ plots. Here we will take $n=0.5$ as these are direct band gap semiconductors. From the plots the value of band gap value E_g for pure and different weighted doped samples were calculated and summarized in Table 1. The modifications in band gap with different atomic wt% of Pb in InSe glasses were graphically shown in Fig. 5.

Table 1. Variation in bandgap with doping concentration

Sr. No.	Sample	Band gap (E_g) eV
1.	Pure InSe	1.72
2.	(InSe)Pb ₂	1.69
3.	(InSe)Pb ₅	1.67
4.	(InSe)Pb ₁₀	1.55

The changes in band gap (E_g) with different weighted Pb concentrations are displayed in Fig. 5. This variation could be made clear by describing the composition dependent bond energy variation of amorphous film. Pauling suggested [10] that when two atoms A and B with different electronegativity values χ_A and χ_B combine to form a heteronuclear compound then, the mono covalent bond energy of homonuclear D(A-A) and D(B-B) could be used to estimate the bond energy of heteronuclear bond D(A-B) using the relation:

$$D(A-B) = [D(A-A) \times D(B-B)]^{1/2} + 30(\chi_A - \chi_B)^2 \quad (4)$$

The single bond energy values of In-In are 84.5 kJ mol^{-1} , Se-Se is $206.1 \text{ kJ mol}^{-1}$ and Pb-Pb is 85.7 kJ mol^{-1} [11]. Also Allred-Rockow electro-negativity values were made use of, for estimating In-Se and Pb-Se single bond energy values which were found to be $257.5 \text{ kJ mol}^{-1}$ and $231.2 \text{ kJ mol}^{-1}$ respectively. With the addition of Pb in InSe chalcogenide glasses, In-Se bonds were thoroughly replaced by Pb-Se bonds. Since the bond energy of Pb-Se bond is comparatively lower than In-Se bond, the increased concentration of Pb in InSe glasses from 2 at wt% to 10 at wt% would result in more decrease in bond energy of solid. As optical band gap is directly and strongly influenced by bond energy, therefore this decrease in average bond energy would in turn decrease the band gap of the material. Hence a decreasing trend in optical band gap was observed with increasing Pb at wt% whose variation is graphically depicted in Fig. 5.

3.3. Electrical Studies

The electrical characterization of all the four samples namely Pure In₁₀Se₉₀, (In₁₀Se₉₀)₉₈Pb₂, (In₁₀Se₉₀)₉₅Pb₅ and (In₁₀Se₉₀)₉₅Pb₁₀ were performed using two probe method in a sample holder attached to BC2410; British Thomson Houston Ltd. rotary pump for providing a vacuum of the order of 10^{-3} mbar throughout the experiment. All the experiments were performed at room temperature conditions and samples were firstly stabilized for at least one hour under vacuum for removal of impurities from the setup.

3.3.1. Current-Voltage (IV) Characterization

The current-voltage (IV) characterization of all the samples i.e. In₁₀Se₉₀, (In₁₀Se₉₀)₉₈Pb₂, (In₁₀Se₉₀)₉₅Pb₅ and (In₁₀Se₉₀)₉₅Pb₁₀ were performed to check the Ohmic behaviour of the prepared glasses. Here the current values were noted down at voltage range ranging from 0 V to 5 V as shown in Fig. 6. It was found that all the samples exhibited Ohmic behaviour but the maximum current was found in the case of (In₁₀Se₉₀)Pb₁₀ i.e. with 10 at wt% Pb doped InSe nanoparticles. This increase in current may be due to modifications of defect states which results in increase in number of charge carriers and enhanced the current values [12].

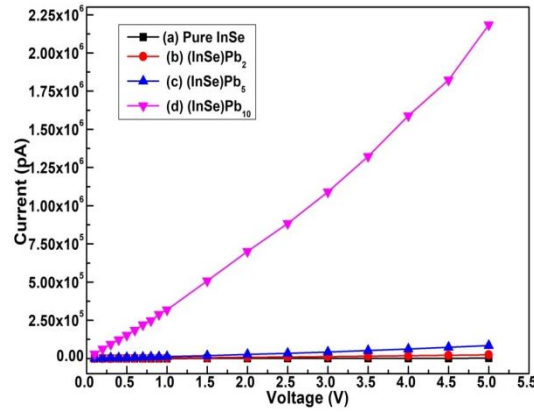


Fig.6. IV characteristics of Pure $In_{10}Se_{90}$, $(In_{10}Se_{90})_{98}Pb_2$, $(In_{10}Se_{90})_{95}Pb_5$ and $(In_{10}Se_{90})_{95}Pb_{10}$.

3.3.2. Dielectric measurements

Fig. 7 shows the variation of real and imaginary parts of dielectric constant as a function of frequency tuned from 50 Hz to 5 MHz for $In_{10}Se_{90}$, $(In_{10}Se_{90})_{98}Pb_2$, $(In_{10}Se_{90})_{95}Pb_5$ and $(In_{10}Se_{90})_{95}Pb_{10}$. Here the variation of capacitance (C) and conductance (G) with varying frequency were taken at room temperature and then different parameters such as real part of dielectric constant (ϵ'), imaginary part of dielectric constant (ϵ'') and dielectric loss ($\tan\delta$) were calculated using the following relations [13]:

$$\epsilon' = \frac{C}{C_0} = \frac{Cd}{\epsilon_0 A} \quad (5)$$

$$\epsilon'' = \frac{G}{\omega C_0} = \frac{Gd}{\omega \epsilon_0 A} \quad (6)$$

Where d is thickness of sample (cm), A is sample area (cm^2), ϵ_0 is permittivity of free space ($= 8.854 \times 10^{-14} F cm^{-1}$), C_0 is capacitance of empty capacitor ($C_0 = \epsilon_0 d/A$) and ω ($= 2\pi f$) is angular frequency of applied electric field.

The dielectric loss expressed in terms of $\tan\delta$ can be calculated as [14]:

$$\tan\delta = \frac{\epsilon''}{\epsilon'} = \frac{G}{\omega C} \quad (7)$$

The obtained values of ϵ' , ϵ'' and $\tan\delta$ using eqns. (5), (6) and (7) for various frequency range were calculated and are displayed in Fig. 7(a), 7(b) and 8 respectively.

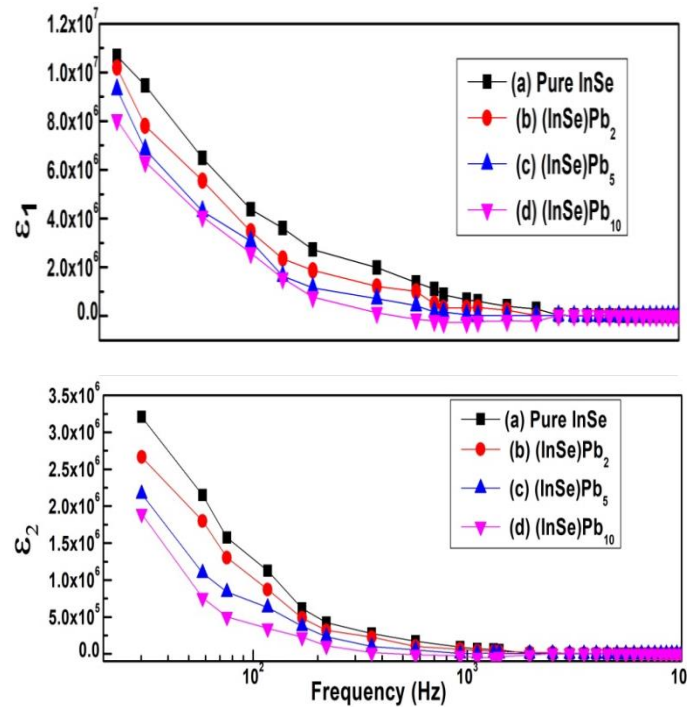


Fig.7. Plots of real (ϵ_1) and imaginary parts (ϵ_2) of dielectric constants vs frequency (ν).

From Fig. 7 it is clearly observed that with increase in frequency real as well as imaginary part of dielectric constant, both follow a decreasing trend. However there is a negligible change in the values at higher frequency regime. Maxwell-Wagner and Koops nomenclature theory [15] could be used for better explanation of the frequency dependent behaviour of dielectric constant. According to this model, incompetently conducting grain boundaries are well separated by number of well distributed conducting grains. At low frequencies, grain boundaries play predominant role while at high frequencies the conducting grains have the major role to play. In actual, it is the contribution of surface charge polarization towards dielectric constant variations at low frequencies. This is due to accumulation of surface charge carriers under the effect of applied electric field. When frequency value increases, the change in electric field values occurs very fast and results in lagging of electrons behind the electric field as they were unable to keep in phase with applied electric field. This electron lagging reaches the grain boundary as well as completely spread over the whole domain and results in decrease in value of dielectric constant at high frequencies. However with doping of chalcogenide glasses InSe with Pb shows that with increasing Pb contents, ϵ' and ϵ'' shows decrease in values which may be due to modification of defects states which further increase the number of charge carriers.

The dielectric loss ($\tan\delta$) as shown in fig.8 also follow similar trend with comparatively lesser loss observed at maximum doping values i.e. $(\text{In}_{10}\text{Se}_{90})\text{Pb}_{10}$ with 10 at. wt % of Pb. This dielectric loss may be attributed to the combine effect of impurities, space charge formation between various interfacial layers and various defects which results in absorption current generation and causes dielectric loss [16].

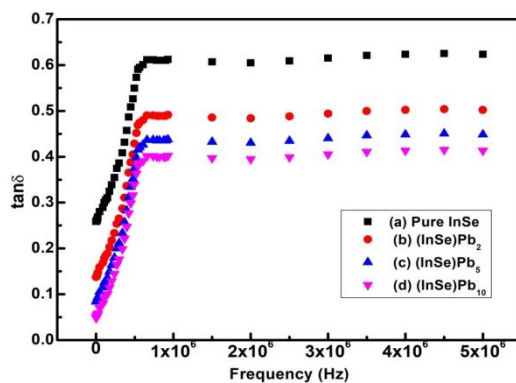


Fig.8. Plot of dissipation factor ($\tan\delta$) vs frequency (ν).

4. Conclusions

In summary, pure InSe and different weighted Pb doped chalcogenide glasses had been successfully prepared using conventional melt and quench procedure. XRD results confirmed with the addition of Pb in InSe system, the amorphous nature of the sample was converted into crystalline and the degree of crystallinity was further enhanced with increase in at. wt% of Pb. FE-SEM micrographs revealed that pure InSe particles were spherical in size but with the addition of Pb resulted in the shape distortion and maximum distortion which actually resulted in agglomeration was observed at maximum at. wt% addition i.e. at 10 at. wt%. The band gap of Pure as well as doped InSe glasses was calculated from UV-Vis studies.

It was observed that with increase in Pb content, the band gap value followed a decreasing trend from $E_g = 1.72$ eV in the case of pure InSe to $E_g = 1.55$ eV in the case of (InSe)Pb₁₀ with 10 at. wt % of Pb. The electrical characterization of all the samples was performed at room temperature along with dielectric measurements for studying dielectric properties. Various parameters such as real and imaginary parts of dielectric constant i.e. ϵ' and ϵ'' respectively along with dielectric loss values were calculated with varying frequency ranging from 50 Hz to 5 MHz.

References

- [1] R. Frerichs, J. Opt. Soc. Am. **43**, 1153 (1953).
- [2] A. Ray Hilton, Appl. Opt. **5**, 1877 (1966).
- [3] A. Kumar, M. Lal, K. Sharma, S. K. Tripathi, N. Goyal, Ind. J. Pure and Appl. Phys. **51**, 251 (2012).
- [4] A. Kumar, M. Lal, K. Sharma, S. K. Tripathi, N. Goyal, chalc. Lett. **9**, 275 (2012).
- [5] Manish Dev Sharma, Jashangeet Kaur, Ankush, Kanika, Navdeep Goyal, International Conference on Inter Disciplinary Research in Engineering and Technology **01**, 51 (2016).
- [6] Manish Dev Sharma, Jashangeet Kaur, Ankush, Kanika and Navdeep Goyal, International Journal of Engineering Sciences **17**, 364 (2016).
- [7] Atsufumi Hirohata, Jagadeesh S. Moodera, Geetha P. Berera, Thin Solid Films **510**, 247 (2006).
- [8] Abolanle S. Adekunle, Seonyane Lebogang, Portia L. Gwala, Tebogo P. Tsele, Lukman O. Olasunkanmi, Fayemi E. Omolola, Diseko Boikanyo, Ntsoaki, Mphuti, John A.O. Oyekunle, Aderemi O. Ogunfowokan, Eno E. Ebenso, RSC Adv. **5**, 27759 (2015).
- [9] Kriti Sharma, Alaa S. Al-Kabbi, G.S.S. Saini, S.K. Tripathi, Materials Research Bulletin **47**, 1400 (2012).
- [10] L. Pauling, The nature of Chemical Bond **3** (1967).
- [11] A. K. Pattanaik, A. Srinivasan, Journal of Optoelectronics and Advanced Materials **5**, 1161 (2003).

- [12] A. V. Kolobov, *J. Non-Cryst. Solids* **728**, 198 (1996).
- [13] S. Demirezen, A. Kaya, S.A. Yeriskin, M. Balbas, I. Uslu, *Results in Physics* **6**, 180 (2016).
- [14] I.M. Afandiyeva, S. Demirezen, S. Altındal, *J. Alloys Compd.* **552**, 423 (2013).
- [15] Zaretsky, Eugene & Kanel, *Journal of Applied Physics.* **112**, 1 (2012)
- [16] M. Md. Hoque, A. Duta , S. Kumar , TP. Sinha, *J. Mater. Sci. Technol.* **30**, 311 (2014).